J Mater Sci (2015) 50:3434–3446
DOI 10.1007/s10853-015-8902-7

Mechanical properties of chromium–chromium sulfide cermets fabricated by self-propagating high-temperature synthesis

Atefeh Nabavi · Samuel Goroshin · David L. Frost · Francois Barthelat

Received: 28 August 2014 / Accepted: 9 February 2015 / Published online: 21 February 2015

Abstract Metal sulfides are widely used in a variety of applications requiring high hardness and toughness. In this study, the microstructure and mechanical properties of chromium–chromium sulfide cermets are investigated. The chromium–chromium sulfide cermet was manufactured using self-propagating high-temperature synthesis, a process where the material is created under a self-sustaining combustion reaction between the chromium and sulfur. This type of synthesis allows the creation of near-net shape structures and offers the possibility of tuning material properties and material behavior by changing the composition of the reactant. Microstructural characterization was performed using optical microscopy, scanning electron microscopy, and energy dispersive spectroscopy. The mechanical properties of the cermet (Young's modulus, fracture toughness, flexural strength, and microhardness) have been measured and related to morphology and chemical composition of the samples. Results show that dense cermets (about 7 % porosity) with specific structure have been obtained. Pure CrS has a significant hardness, but its toughness was insufficient for tool applications. However, we found that the density and fracture toughness of the cermets increase with the addition of Cr. The addition of Cr also improved the flexural strength and hardness of the cermet by 60 % and almost 38 %, respectively.

Introduction

Engineering ceramics are attractive materials because of their low density, high compressive strength, and hardness. However, their use in actual applications is currently limited by their brittleness, fragility, and poor toughness. A possible approach to toughen ceramics is the inclusion of a metallic ductile phase. Such ceramic–metal compounds, called cermets, combine the hardness and stiffness of ceramics with the toughness and ductility of metals [1–5]. Among cermets, metal sulfide composites are in high demand in the chemical, metallurgical, and electrical industries because of their valuable characteristics such as hardness, semi-conductivity, electroluminescence, infrared transparency, catalytic, and magnetic properties [6–9]. Currently, metal sulfides are used for cathodes in batteries, additives in steel production, high-temperature lubricants, catalytic material for hydro-desulfurization, electrodes for hydrogen fuel cells, and solar energy conversion into electric and chemical energy [7, 10–16]. There is currently no bulk production of chromium sulfide, however, we know from the literature that chromium sulfide has magnetic properties, and already is used as a catalyst in chemical processes, and as a solid lubricant [7, 17–19]. Metal-sulfur compositions, such as CrS are attractive in that they offer the possibility of fabrication using the self-propagating high-temperature synthesis (SHS) technique.

In a previous study, we used a new method for the preparation of the metal-sulfur precursor charge based on the ability to melt-cast the precursor mixture [20]. We used SHS to produce a chromium–chromium sulfide cermet, using the ability of the metal–sulfur mixture to support the propagation of reactive waves. This ability, with the properties of the reaction products (i.e., low gas evolution

---

Electronic supplementary material The online version of this article (doi:10.1007/s10853-015-8902-7) contains supplementary material, which is available to authorized users.

A. Nabavi · S. Goroshin · D. L. Frost (✉) · F. Barthelat (✉)
Department of Mechanical Engineering, McGill University,
817 Sherbrook Street West, Montreal, QC H3A 0C3, Canada
e-mail: david.frost@mcgill.ca

F. Barthelat
e-mail: francois.barthelat@mcgill.ca

and liquid sulfide products), enable the possibility to perform net-shape synthesis of dense, near theoretical density product with a relatively simple and low-cost setup [20]. This novel method simplifies the preparation of samples with different shapes, thicknesses, and with a green density close to the theoretical density. It also improves the quality of the synthesized product, and homogeneity of the product structure [1, 7, 21, 22].

While the thermochemical calculations predict near-zero gas production for the chromium-sulfur system, the actual cermets exhibited a large amount of porosity (about 70 %) when synthesized at atmospheric pressure. With the various improvements to the manufacturing process, the porosity was reduced by an order of magnitude from 70 to 7 % [20]. The level of porosity obtained (approximately 7 % for the best samples) is considerably less in comparison to samples produced by other SHS techniques and is comparable to the bulk form of industrially manufactured ceramics [23].

In the present study, we first estimate the mechanical properties of the fabricated cermets and evaluate the effect of the improvements applied to the combustion manufacturing process ("Effect of manufacturing process" Section). Then, we attempt to improve the toughness and other mechanical properties of the Cr–CrS cermets by increasing the metal content. The mechanical properties are measured as a function of Cr:S molar ratio and the results obtained demonstrate that the addition of Cr has a significant influence on the mechanical properties.

One of the advantages of this type of synthesis is that it offers the possibility of tuning material properties and material behavior by changing the reactant composition. In particular, it is in theory possible, by systematically increasing the Cr content in the precursor mixture, to tune the final product from a brittle ceramic to a more ductile metal-like material. In other words, the ductility of the Cr–CrS cermet can be controlled through the variation of the Cr:S molar ratio in the reactive mixture, enabling the cermet to contain an excess of chromium in the final product to increase ductility. Although equilibrium thermodynamic calculations predict that 200 % excess Cr is the upper limit on the Cr content for a self-sustained reaction to occur [24], this study stopped at a Cr:S ratio of 4 times stoichiometric in order to find the maximum Cr content that could be added to the produced cermet. All thermodynamic calculations were carried out using the FactSage thermochemical software [25].

Materials and manufacturing process

The preparation of the reactive mixture used in this study is straight forward and can be explained in few steps. The chromium powders were obtained from Atlantic Equipment Engineers (NJ, USA), with a purity of 99.8 %, and with particle size ranges of 1–5 μm (CR-102) and <44 μm (CR-103). The particle size distribution of the Cr powders, measured with an LA-920 Horiba laser scattering particle size analyzer shows the CR-102 and CR-103 powders had average particle sizes, based on volume, of 3 and 26 μm, respectively. Sulfur powder with a purity of 99.5 % was obtained from Alfa Aesar (S4981, MA, USA). The average particle size was smaller than 150 μm (−100 mesh) but did not influence the fabrication process, since the sulfur was always melted to form the reactive mixture.

As a first step, samples were synthesized at atmospheric pressure. These fabricated samples generally had high porosity, including both micro- and macro-cracks. To reduce the porosity and the number of cracks that form in the product, a modified manufacturing process was used, which is described below.

Chromium and sulfur powders were mixed in a roller mill with the desired mass ratio. The powder mixture was then heated in a mantle up to a temperature slightly above the melting temperature for sulfur (i.e., temperature > 120 °C), but well below the melting temperature of chromium (1907 °C). Adsorbed water, low boiling-point impurities, and dissolved hydrogen on the surface of powders prior to SHS, are possible sources for impurity-generated porosity in SHS products. Due to the high combustion temperatures, these impurities are volatilized as the wave propagates through the reactants during the SHS process. Therefore, the best way to reduce these sources of porosity is to use highly purified initial powders which can eliminate or significantly reduce the formation of impurity-generated porosity, as well as vacuum degassing the molten mixture to remove trapped gases before ignition. The molten mixture of Cr and S powders was degassed in a vacuum chamber (pressure = 95 kPa) for about 20 min and at high enough temperature (160 °C) to maintain sulfur in the molten state. After that, the mixture was poured into a preheated cylindrical steel mold (2.5 inches in diameter and 4 inches in height) at a temperature near the melting point of sulfur to prevent contact solidification of the melt. Upon cooling of the reactive mixture the sulfur solidified, forming a matrix of sulfur containing well-dispersed chromium inclusions. Figure 1 contains an SEM micrograph of the reactive mixture showing chromium particles (lighter regions) uniformly dispersed within the solidified sulfur matrix (darker regions). The solidified reactive mixture was then placed in a pressurized reactor and ignited inside the mold under a high-pressure inert gas (Ar) environment, by using an electrically-heated tungsten wire embedded in the sample.

There were many micro- and macro-cracks in the first samples produced. These cracks may be due to thermal

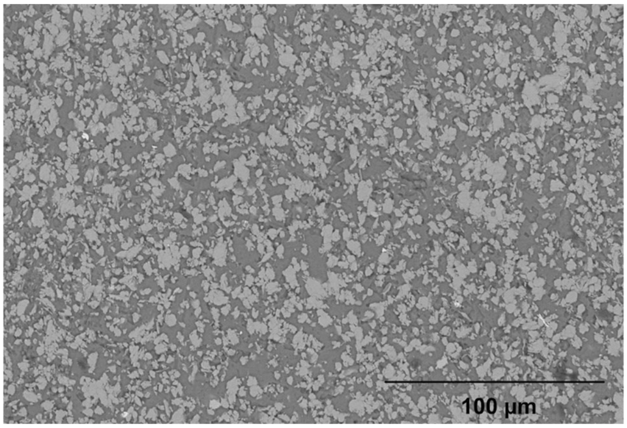

Fig. 1 SEM micrograph of the reactive mixture showing chromium particles (*light tone*) embedded in solidified sulfur matrix (*darker tone*). The distribution of the chromium particle was uniform

shock resulting from the high cooling rate of the product (10^3–10^6 °C/min) and the contraction of the mixture as it solidifies. As a result, a shrinkage defect will form when the solidification is governed by progressive solidification from the outer surface of the sample towards the sample interior. Therefore, in order to prevent cracks and voids from developing, we developed a method to cool the samples slowly and directionally after the reaction. Directional solidification is achieved by a one-dimensional thermal flux along the sample axis and sufficient heat exchange between the sample and cooling medium. Figure 2 shows a schematic of the directional solidification method in which a jacket of SHS mixture was cast on top of a shallow layer of inert ceramic. This prevented heat loss from the top of the sample, while allowing a small amount of heat to transfer through the inert ceramic, and a greater amount of energy to escape through the base of the steel mold. The solidification front therefore moves in a unidirectional manner from bottom to top. This modification successfully suppressed crack formation. The self-sustained flame propagated throughout the sample, producing the final metal sulfide product. Depending on the initial metal/sulfur molar ratio, the amount of unreacted metal remaining in the product varies, enabling the final product to range from a brittle ceramic to a more ductile metal-like material.

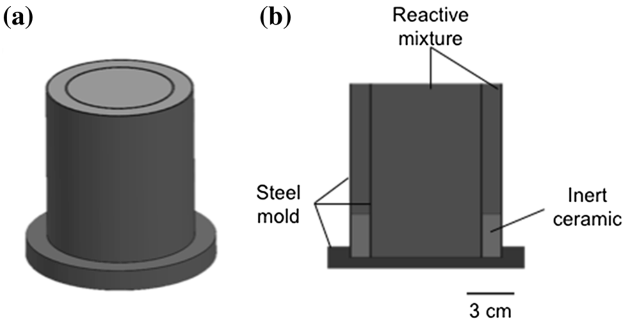

Fig. 2 **a** Schematic representation of directional solidification method, **b** sectional view

By igniting the sample above the liquid–vapor critical point of sulfur and cooling the samples slowly and directionally, the cermet sample produced had a porosity of about 7 % and no cracks were formed within the product. After the cylindrical cermet sample was cooled to room temperature, it was removed from the mold. The modified manufacturing process is shown schematically in Fig. 3.

Structural and microstructural characterization

To investigate the microstructure of the samples produced, including the morphology, size, distribution, and composition of the different phases, the specimens were cut, polished, and examined with scanning electron microscopy (Hitachi S-3000N VP-SEM), optical microscopy, and energy dispersive spectroscopy (EDS). The volume fractions of voids and the different phases within the specimens were estimated by performing image analysis on backscattered electron images (BSE) and optical microscopic images, based on the ASTM E 562-02 standard test method for determining volume fraction by systematic manual point count [26]. By analyzing the backscattered images taken by SEM and using a quantification feature in the Clemex image analysis software package, the volume fractions of different phases were extracted as statistical data. The atomic masses of chromium, sulfur, and chromium sulfide are significantly different from each other, and therefore these species may be easily identified in backscattered images.

X-ray diffraction (XRD) was used to determine the nature of the different phases which were formed during the synthesis or post-ignition process. Combustion-synthesized products with a Cr:S molar ratio 1:1.3 were ground into fine powders and analyzed using Cu Kα1 X-ray radiation to assess the phase constituents. XRD analyses showed Cr and CrS peaks (Fig. 4c).

Density

The density of the samples after the reaction was measured. The relative density of the Cr–CrS cermets, obtained by the Archimedes method, varied between 83 and 110 % of the theoretical density of CrS, for an initial Cr:S molar ratio of 1.15:1–4:1, respectively. Additionally, the pores were small and uniformly distributed throughout the cermets

Fig. 3 Schematic of the modified manufacturing process

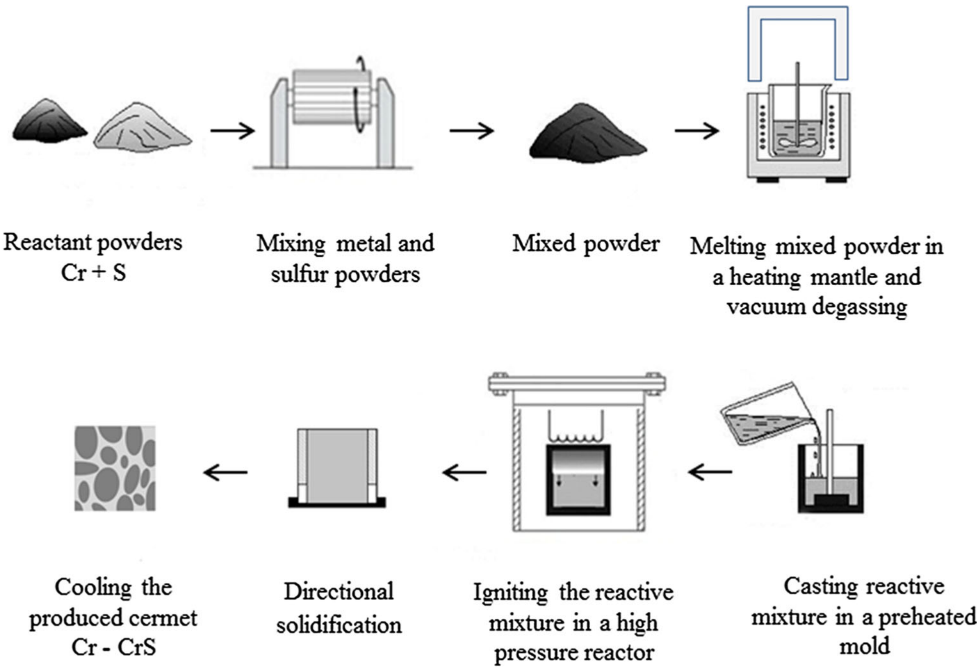

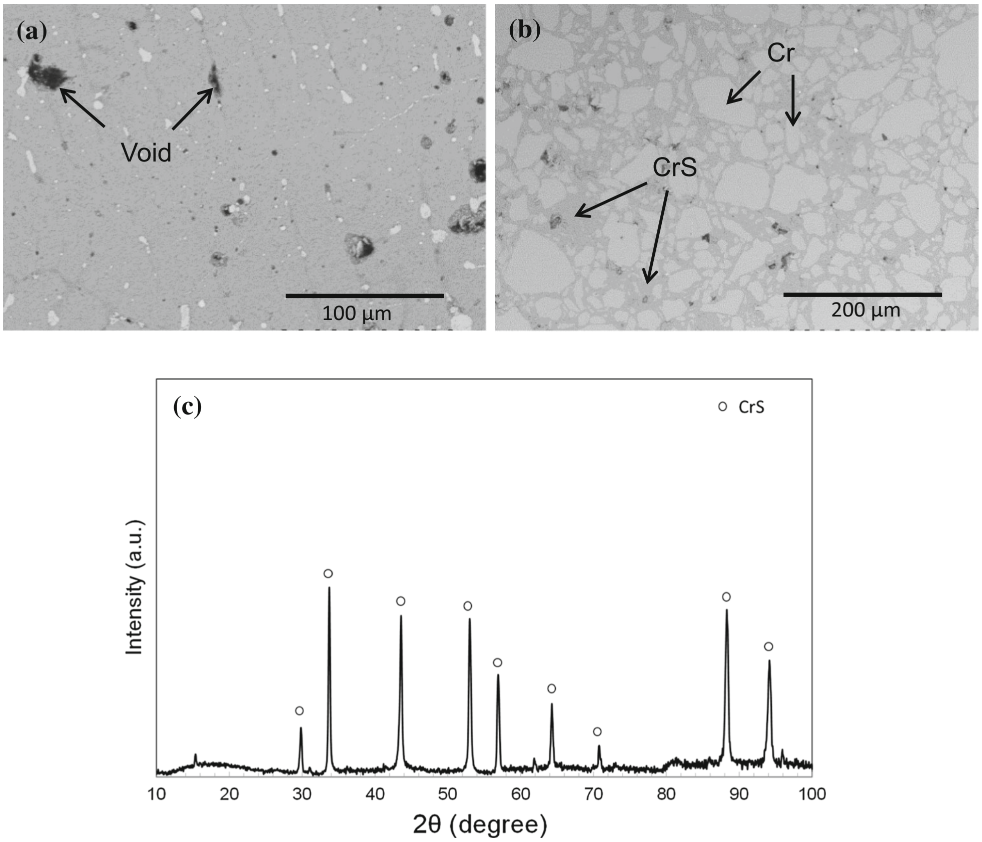

Fig. 4 Backscattered images of produced samples each with Cr:S molar ratio equal to; **a** 1.15:1, and **b** 4:1 sample. *Light regions* are residual Cr phase, *dark gray regions* are chromium sulfide, and *black regions* correspond to voids; **c** XRD pattern of samples fabricated with Cr:S molar ratio 1:1.3

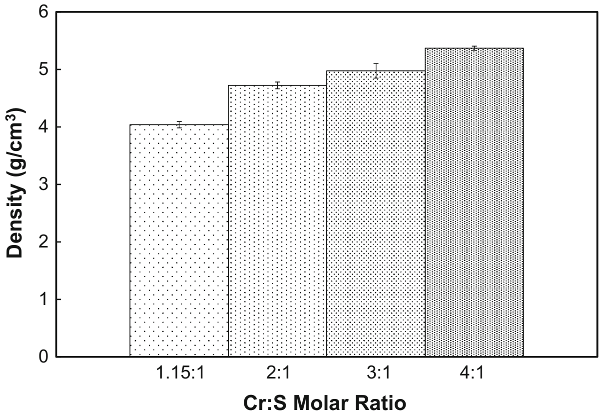

Fig. 5 Density of cermets produced as a function of Cr:S molar ratio

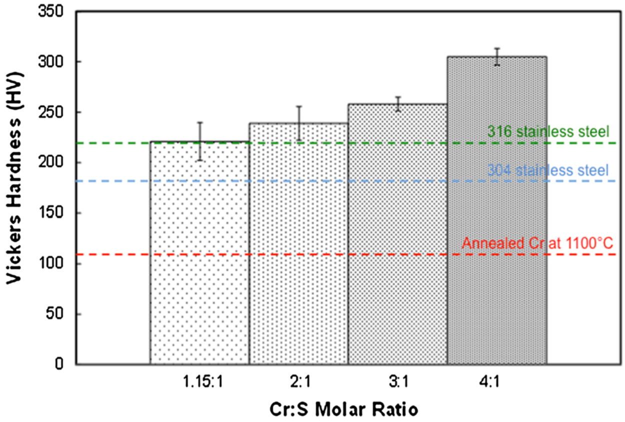

Fig. 6 Hardness of cermets produced as a function of Cr:S molar ratio

produced. The density of Cr is higher than that of CrS and Cr_2S_3 and, as expected, cermet density increases from 4.04 ± 0.05 to 5.37 ± 0.04 g/cm^3 as the Cr content was increased from 115 to 400 %, respectively (see Fig. 5).

Microhardness

In order to measure the microhardness of the synthesized samples, the samples were cut and fixed in epoxy, then polished with a 3-µm diamond paste, and then cleaned with ethanol. Microhardness measurements of the matrix of the cermets produced were made using a BUEHLER 2101 Vickers microhardometer, and the hardness test was performed under an indentation load of 50 gf for 20 s. Analysis points were sufficiently spaced to eliminate the effect of neighboring indentations. Indents were made on the porosity-free areas, and any distorted indents indicating entrapped pores were discarded from the measurements. An average of 10 indentations was performed on each sample cross section and the values are reported in Fig. 6.

Figure 6 shows that the microhardness increases with increasing Cr content within the reactive mixture. Based on the CrS phase diagram [27] and XRD results, the chromium solute content (solid solution) of these cermets can contribute to the hardness improvement. One-way ANOVA exhibited a significant difference ($p < 0.005$) among the tested cermet materials for the mean values of microhardness. As can be seen in Fig. 6, the hardness is measured to range from 221 ± 18 to 305 ± 8 HV, for Cr:S 1.15:1 and 4:1 molar ratios, respectively. For comparison, the hardness of annealed chromium at 1100 °C is 110 HV, chromium that is extruded, annealed, and rolled at 400 °C is 160 HV, 304 stainless steel is 183 HV, and 316 stainless steel is 220 HV [3].

Three-point bending

For the three-point bending test, specimens were prepared by cutting the fabricated cermet into small-sized beam-type prisms with a length of 20 mm and rectangular cross section of 4 × 4 and 2 × 4 mm, using a high-precision diamond saw (Fig. 7a). The loading stage and sample were placed under an optical microscope (BX-51M, Olympus, Markham, Canada) equipped with a CCD camera (RETIGA 2000R, Qimaging, Surrey, Canada) to capture crack propagation, as shown in Fig. 7b, c. The quasi-static mechanical tests were performed using a three-point bending fixture mounted on a miniature loading stage (Ernest F. Fullam Inc., Latham, NY). The specimens were loaded at a rate of 0.0025 mm/s up to complete failure. For each composition, six different test samples were used. One-way ANOVA showed that flexural strength was significantly affected by Cr content in fabricated cermets ($p < 0.01$). As can be seen from Fig. 8, the flexural strength increases from 444 to 727 MPa as the Cr:S molar ratio increases from 1.15:1 to 4:1, respectively. The Young's modulus also increases with increasing Cr content in the cermets produced. The stiffest material achieved had a Young's modulus of 186 ± 14 GPa for the cermet with Cr:S 4:1 molar ratio (Fig. 9).

Fracture toughness

Fracture toughness tests were performed using a three-point bending fixture with a span of 16 mm, mounted on the same miniature loading stage (Ernest F. Fullam Inc., Latham, NY). The loading stage and sample were placed under an optical microscope and the specimens were loaded at a rate of 0.0025 mm/s up to complete failure. Samples were prepared by cutting the cermet specimen into

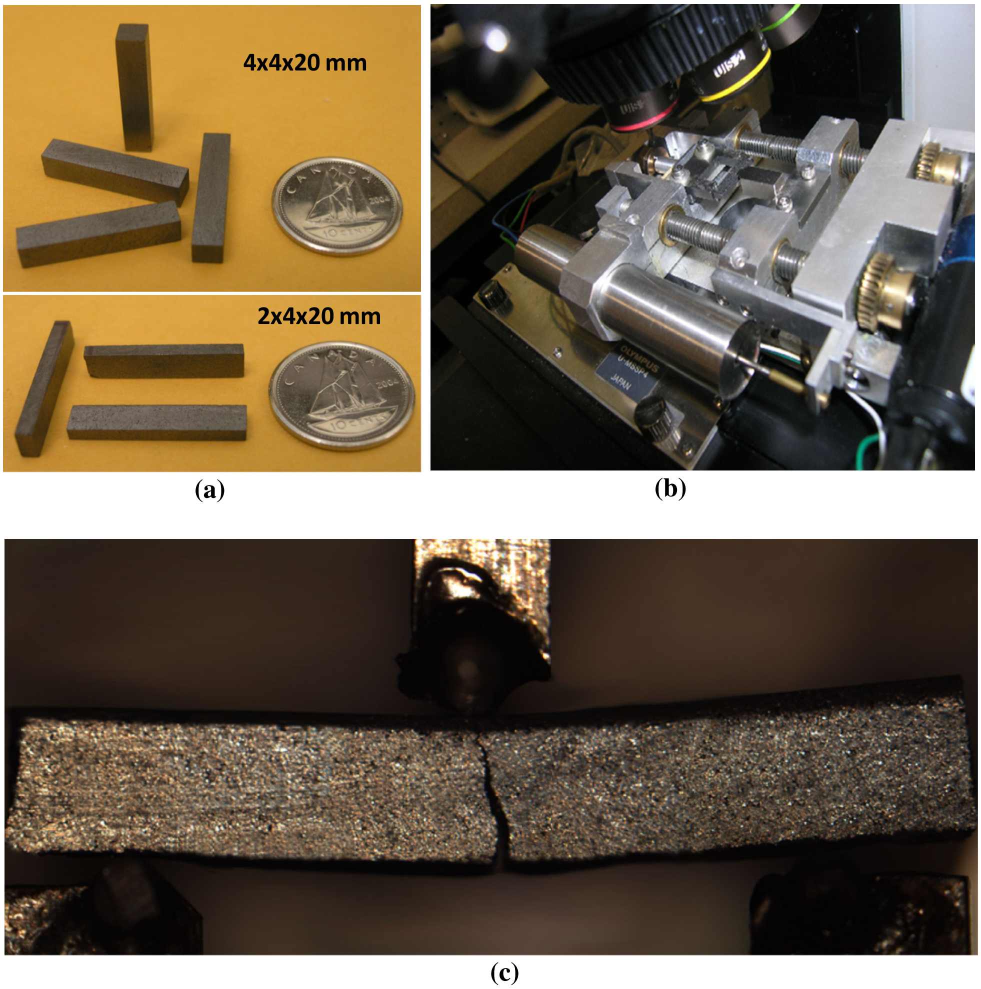

(a)
(b)
(c)

Fig. 7 **a** Samples for three-point bending test, **b** photograph of test setup, and **c** crack propagation along the cermet sample

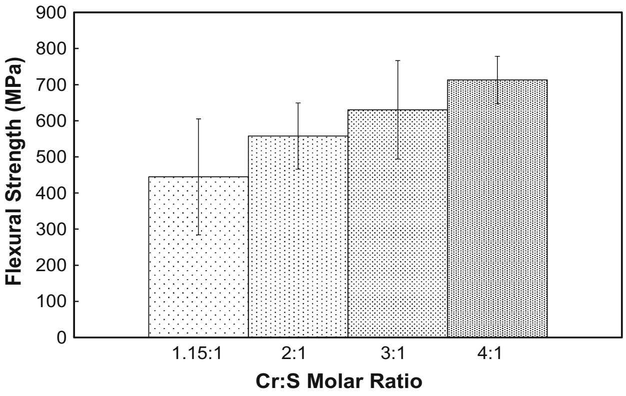

Fig. 8 Flexural strength of produced cermets as a function of Cr:S molar ratio

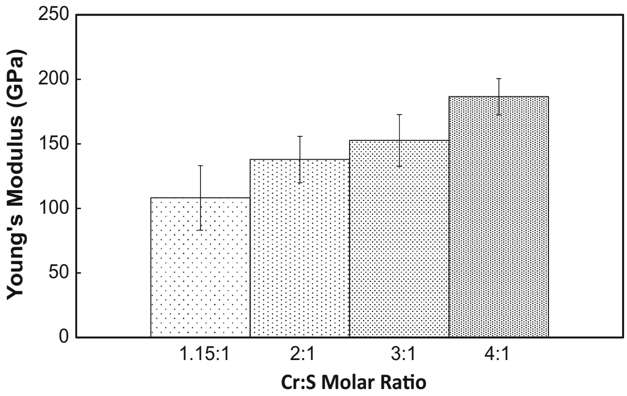

Fig. 9 Young's modulus of produced cermets as a function of Cr:S molar ratio

small beam-shaped pieces with a length of 20 mm and a rectangular cross section of 2 × 4 mm, using a high-precision diamond saw. The samples were then pre-notched using the diamond saw. One side of the specimen was polished and the notch was deepened and sharpened with a razor blade. The notch depth was about 2.0 mm, which was within 45–55 % of the width in order to comply with the ASTM E1820-01 standard test method for measurement of fracture toughness, as shown in Fig. 10b. For each composition, six different test samples were used.

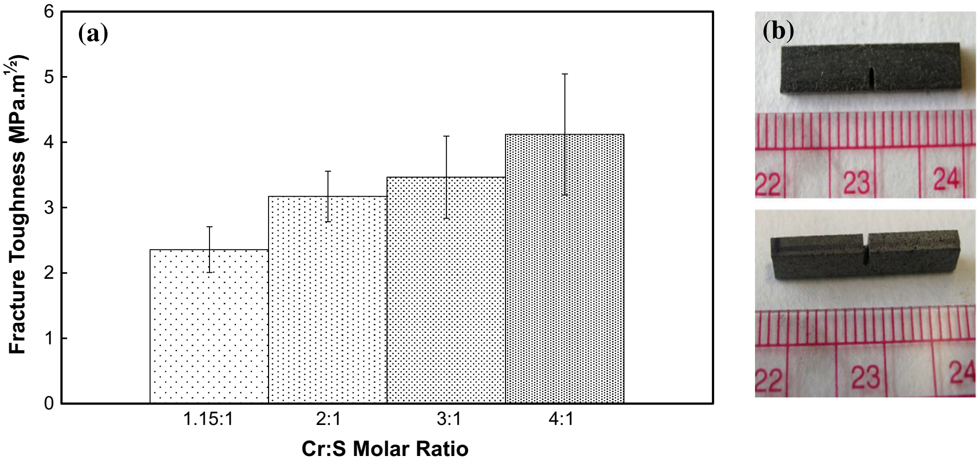

Fig. 10 **a** Fracture toughness of synthesized cermets as a function of Cr:S molar ratio, and **b** samples for fracture test

One-way ANOVA revealed a significant influence of the Cr:S molar ratio on the fracture toughness values of the cermets produced ($p < 0.05$). Figure 10a shows that increasing the Cr content from a Cr:S molar ratio 1.15:1 to 4:1 improved the fracture toughness of the cermet by almost 75 %.

Fracture surfaces

Figure 11 shows the fractured surfaces of the flexural samples. The microstructure of the specimens was examined using SEM on fresh fractured surfaces, containing the remaining Cr particles and the chromium sulfide phase. Secondary electron (SE) and backscattered electron (BSE) images of each surface are shown in Fig. 11. The combination of these two imaging modes provides valuable and complementary information, i.e., the SE mode focuses on image topography, and the SE image has relatively good resolution and provides more detail regarding the surface morphology. In contrast, in the backscattered electron image of the same fracture surface, the surface texture is less obvious. However, a difference in contrast is now visible between the Cr and CrS phases. Since the intensity of the BSE signal is strongly dependent on the mean atomic number of the compound, BSE images contain compositional information, and because heavier elements with a high mean atomic number backscatter more efficiently, they appear brighter than lighter elements in a BSE image [28]. Therefore, the white phase in the BSE images corresponds to areas of Cr which has the highest atomic numbers, whereas the phase with a gray appearance would be CrS which has a lower atomic number.

From an examination of Fig. 12, which shows a fracture path in a 4:1 Cr:S molar ratio cermet, it is apparent that the fracture path passes directly through the Cr particles. A few secondary cracks can be seen in some Cr particles and these are indicative of the brittle nature of the Cr particles. The interface plays an important role in the fracture behavior of cermets. If the fracture strength of the matrix is greater than that of the Cr particles, as in this case, the Cr particles crack when the magnitude of the local stress exceeds the particle fracture strength. This points to the fact that particle breakage has taken place during the fracture process and is characteristic of a strong Cr particle-CrS matrix bond.

From a physical point of view, a certain amount of ductility in the reinforcement can cause a significant improvement in the toughness of brittle matrix composites. It has also been recognized that for achieving an improvement in the fracture toughness, the matrix–reinforcement interfacial strength is as important as the ductility of the reinforcing phase, and the ductility of the reinforcing phase alone is not sufficient. For example, if the interface is very strong, a high degree of constraint can lead to a triaxial state of stress, resulting in a brittle failure of the ductile reinforcement. As a result, under these circumstances there would not be a significant increase in the composite toughness [29].

SE images show relatively featureless, flat surfaces suggesting little or no plastic deformation. Brittle or non-ductile (also called semi-brittle) fracture involves little or no appreciable plastic deformation prior to failure. As can be observed, the major toughening mechanism is the partial plastic deformation of chromium particles.

Figure 11 shows typical features of brittle fracture surfaces. In this case, the origin of fracture is usually a surface defect, i.e., porosity, micro-cracks, inclusions, angular-shaped constituent particles, etc. A surface defect will act as a point of stress concentration within the material. The

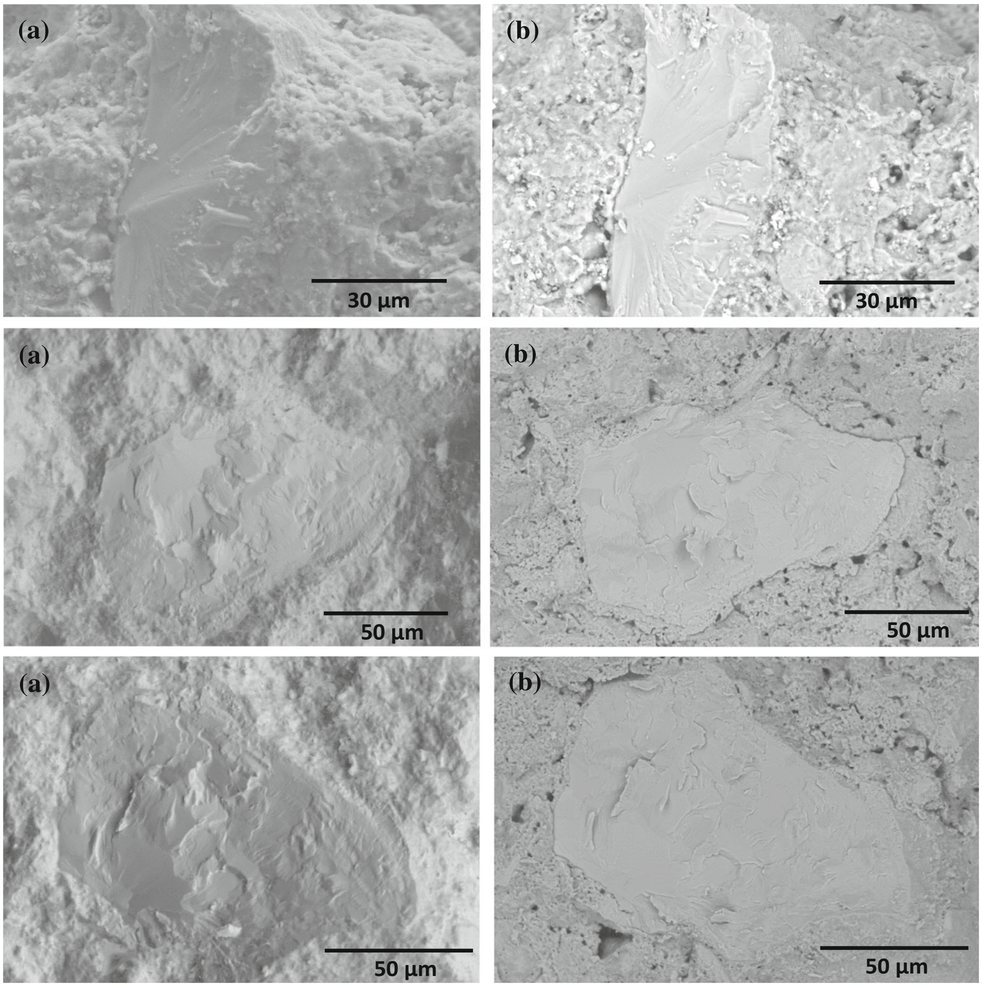

Fig. 11 Fracture surface in a synthesized cermet with a Cr:S molar ratio of 4:1; **a** SE image, and **b** BSE image

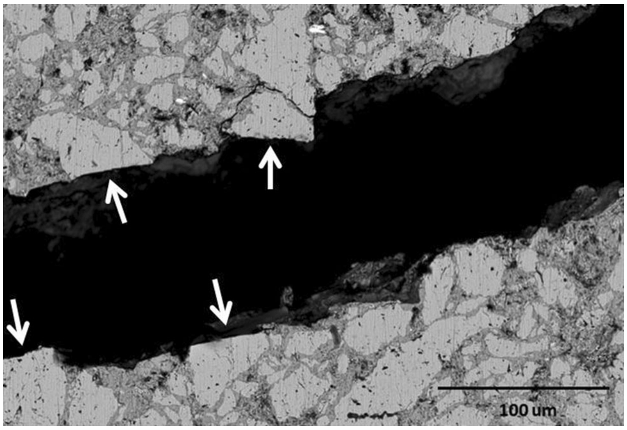

Fig. 12 Fracture path in a synthesized cermet with a Cr:S molar ratio of 4:1

presence of such points of high stress concentration will greatly increase the possibility of brittle failure. Specially, ceramics and glasses have very high yield strengths, and thus very little plastic deformation takes place at crack tips in these materials. Even allowing for a small degree of crack blunting, the local stress at the crack tip is still in excess of the ideal strength and is thus large enough to literally break apart the interatomic bonds there; the crack then spreads between a pair of atomic planes giving rise to an atomically flat surface by cleavage. In the vicinity of regions in these figures, brittle cleavage fracture modes were observed. The fracture surface has a faceted morphology because of the different orientations of cleavage planes in the grains. Cleavage fracture occurs by separation along certain crystallographic planes having low Miller indices [29, 30].

Effect of manufacturing process

Samples synthesized at ambient pressure generally had high porosity (as high as 70 %) with a large number of micro- and macro-cracks. The possible sources of the porosity were considered and as a result the manufacturing process was modified in order to address these issues and minimize the porosity [20]. In the modified manufacturing process the particle size of the reactants was considered. Then, the molten mixture of Cr and S powders was degassed in a vacuum chamber (vacuum pressure = 95 kPa) for about 20 min and at high temperature to maintain sulfur in a molten state. After that, it was poured into a preheated mold to prevent contact solidification of the melt. The solidified reactive mixture was then placed in a pressurized reactor and ignited in a high-pressure inert gas (Ar) environment, by using an electrically heated tungsten wire embedded in the sample. By igniting the sample above the liquid–vapor critical point of sulfur, and cooling the samples slowly and directionally after the reaction, the porosity inside the produced cermets was reduced to about 7 %, and no cracks were observed inside the cermets.

To demonstrate the effect of these improvements in the manufacturing process, we tested one primary sample, which had 18.6 % porosity and contained thermal cracks, as well as one of our final samples produced which had 7 % porosity with no cracks, but with the same composition (i.e., a Cr:S molar ratio of 1.15:1). As can be seen from Fig. 13, the cermets which were fabricated with a Cr:S molar ratio of 1.15:1 and had 18.6 % porosity and thermal cracks, were brittle with a flexural strain less than 1 %, and a flexural strength of 64.55 ± 2.72 MPa. In comparison, the cermets fabricated with the same Cr:S molar ratio, but under the modified manufacturing process, had a flexural strain of around 2 %, and a flexural strength of 444.75 ± 160.5 MPa.

Like the flexural strength test, the same two different samples were tested to measure fracture toughness, i.e., the first cermet sample had 18.6 % porosity with thermal cracks and the second cermet sample had 7 % porosity with no cracks, each with the same Cr:S molar ratio. According to the ASTM standard E1820-01, the fracture toughness of the cermets was determined to be 1.61 ± 0.44 and 2.36 ± 0.35 MPa m$^{1/2}$, respectively (Fig. 14). All the load–deflection curves indicated that the samples behaved linearly near the beginning of the test up to peak values, followed by catastrophic brittle fracture of the samples.

In summary, since materials synthesized with the SHS process typically have a porosity of at least 20 % and contain cracks, the modifications of the manufacturing process lead to a significant reduction in sample porosity at the microstructural level. Furthermore, these improvements to the sample microstructure (for the case of a Cr:S molar ratio of 1.15:1) improved the flexural strength and fracture toughness by 589 and 46 %, respectively.

Ashby diagrams

The Ashby charts are useful in several ways. They condense a large amount of information into a compact form, they display relations between material properties, and they are useful for the identification of optimum materials. Some of the mechanical properties of materials are of primary importance, in engineering design and also in characterizing the material. These include the material density, strength, modulus, and toughness [31]. Therefore, to be able to compare the synthesized Cr–CrS cermets with other materials, the ranges of the property values for this material have been added to some of the Ashby charts. The extension of the bubble-shaped region for Cr–CrS cermets reflects its range of property values, obtained by varying the Cr content.

Many applications and designs look for strength and stiffness at minimum weight. Therefore, one of the most

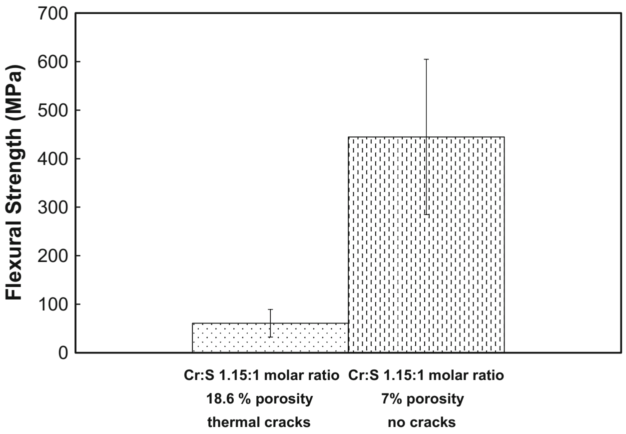

Fig. 13 Flexural strength of synthesized cermets with the same Cr:S molar ratio but a different porosity and presence of cracks (or not) within the cermet

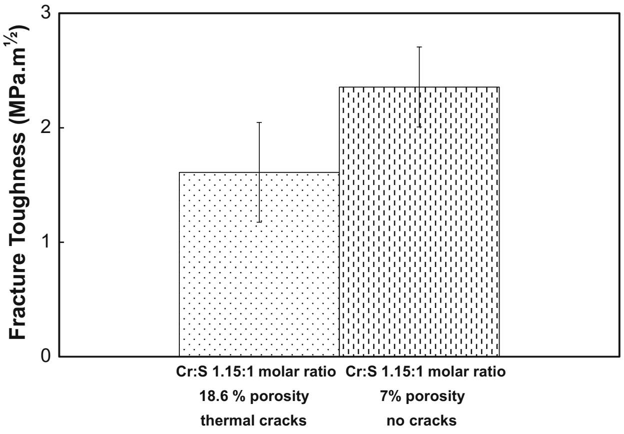

Fig. 14 Fracture toughness of synthesized cermets with the same Cr:S molar ratio but different porosity and cracks within the cermet

useful of all the charts is shown in Fig. 15, which shows E/ρ plotted against σ_f/ρ. In this chart, the word “strength” refers to *yield* strength for metals and polymers, *tear* strength for elastomers, *tensile* strength for composites and woods, and *flexural* strength (modulus of rupture) for ceramics. For all of them, the symbol σ_f is used. These are measures of “mechanical efficiency”, which means the use of the least mass of material to do the most structural work. Composites lie at the upper right. They emerge as the material class with the most attractive specific properties which is one of the reasons for their increasing use. Ceramics have high stiffness and strength per unit weight, but their brittleness excludes them from much structural use. Metals are penalized because of their relatively high densities. Cr–CrS cermets fall on the overlap area between composites and metals which prove that they may perform better than many metals and ceramics in structural applications.

Figure 16 shows another Ashby chart, in which the fracture toughness is plotted against strength. In this chart, the qualifications for “strength” are the same as before. The diagram has applications in selecting materials for the safe design of load bearing structures. Materials toward the top left have high toughness and low strength. Thus, they yield before they fracture. Materials toward the bottom tight do the opposite—they fracture before they yield. Cr–CrS cermets lie on the overlap area between technical ceramics and composites which shows they behave similarly to CFRP, SiC, Al_2O_3, WC, B_4C, etc. in these applications.

Considering these Ashby charts for material selection, it can be concluded that cermets produced in this study can be used in a variety of applications. They can be used as ballistic armors, e.g., composite armor, tank armor, bulletproof vests, and with a metal they can perform as hybrid composite armors. They have the ability to be used in a very wide range of service temperatures, especially at high temperatures since the melting point of chromium and chromium sulfide is higher than 1000 °C. Thus, another application of them is as a refractory material which can be used as heating elements and in high-temperature kilns. They can be used instead of Ti alloys in energy extraction because of their good corrosion resistance and ability to perform in elevated temperature service like Ti alloys. In addition, they have better shear strength and wear properties compared with Ti alloys which makes them suitable for this application. As can be seen from Fig. 17, these cermets are also cheaper than Ti alloys [31, 32].

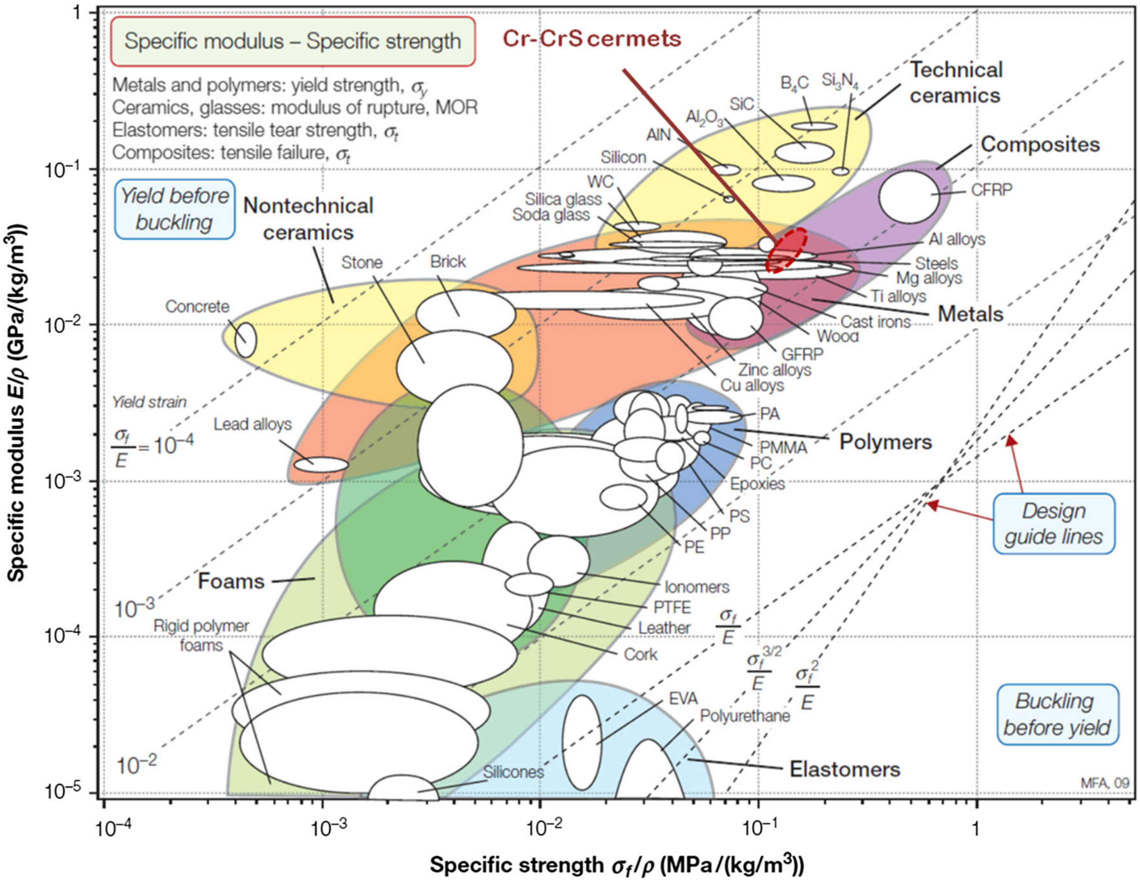

Fig. 15 Specific modulus E/ρ plotted against specific strength σ_f/ρ [31]

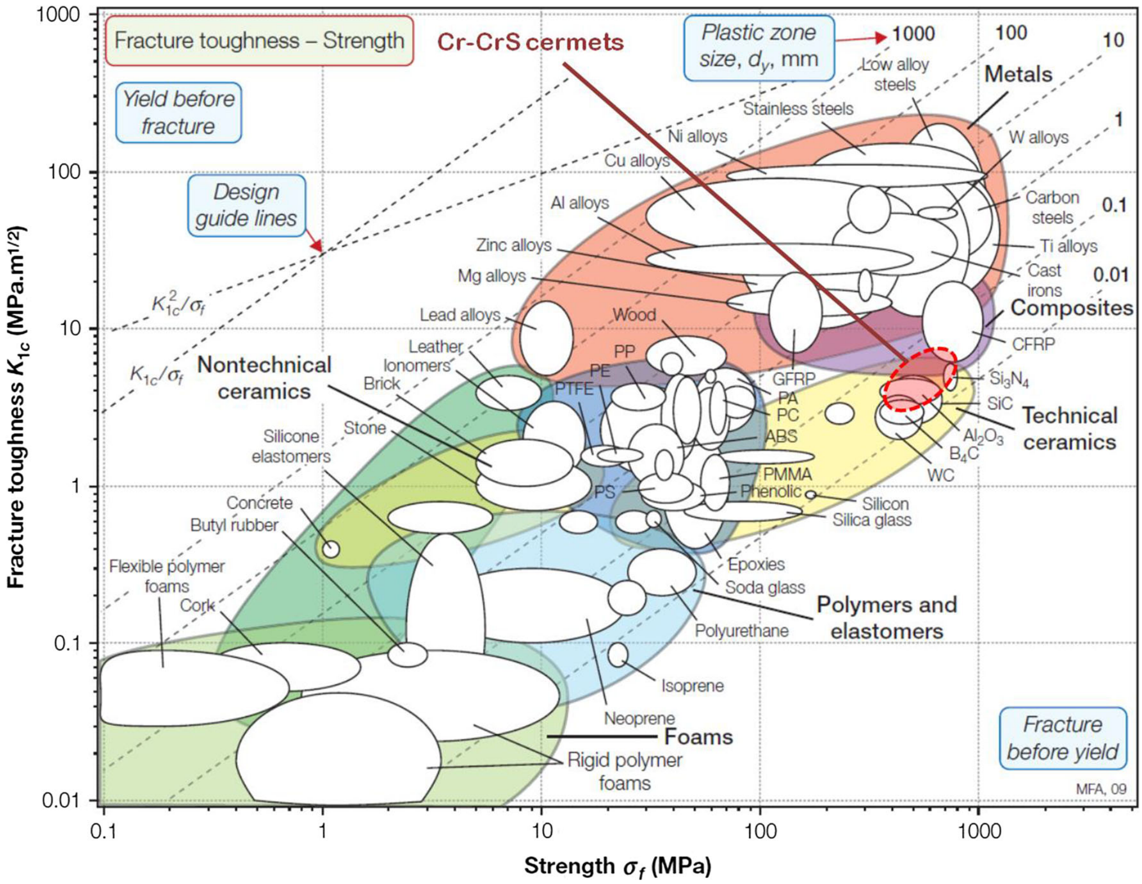

Fig. 16 Fracture toughness K1c plotted against strength σ_f [31]

The cermets produced in the present study can also perform well in a corrosive environment since Cr corrosion resistance is very good. Therefore, Cr–CrS cermets can be used in all applications which involve exposure to seawater or heavy water, such as for parts of ships or naval structures. They can perform as protective coatings to resist corrosion from liquid metals. Therefore, they can replace stainless steel, Ni alloys, and Ti alloys, and furthermore the manufacturing cost of the cermet is lower than these materials. These cermets can be used in the petroleum industry as pipes for natural gas extraction since H_2S gas within natural gas is very corrosive but does not degrade the Cr–CrS cermets. As a result, they can be used in any industry that involves the use of H_2S, such as in facilities for the separation of heavy water from normal water, wastewater treatment plants, and so on. By adding additional metal to the composition, the fracture toughness may be increased. In this case, Cr–CrS cermets can replace Al alloys and steels used in many applications such as the aerospace and automobile industries. The Cr–CrS cermets have the added attraction of having about half the density of steel.

Figure 17 shows the relative cost of different materials based on the latest version of Ashby diagram [31]. The estimated cost of raw materials for producing 1 kg of cermet in the laboratory is about $5–9/kg, with the range in the cost due to differences in the Cr content. As can be seen, in terms of price/kg, the cermet fabricated is between glasses and ceramics (e.g., silicon carbide, alumina, tungsten carbide, etc.). Therefore, in some applications where these ceramics are needed, Cr–CrS cermets can be used instead, because they are more inexpensive, easier to form, faster to produce, flexible in a range of properties.

Conclusions

The aim of this work was to demonstrate the production of dense cermets from original starting powders, to evaluate their physical and mechanical properties, and to correlate them with the chemical composition. This paper has demonstrated the ability of the melt-casting SHS technique developed here to produce near theoretical density chromium/chromium sulfide ceramic–metal composite (cermet) articles of a desired shape. Dense specimens with

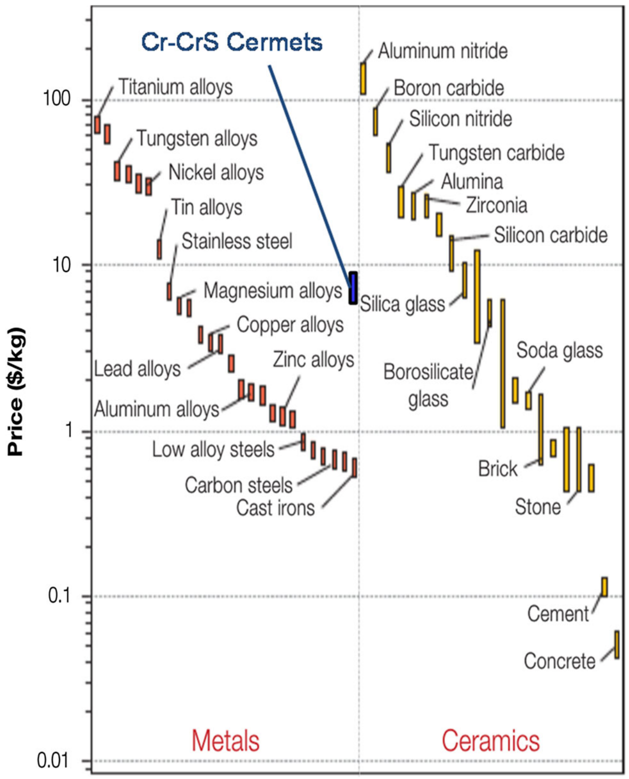

Fig. 17 The approximate price/kg of materials. Commodity materials cost about \$1/kg, special materials cost much more [31]

Cr particles embedded in a chromium sulfide network were obtained.

The microstructure, mechanical properties, and fracture surfaces of CrS-based cermets have been investigated and clearly observed. Also, the influence of Cr addition on the microstructure and mechanical properties of Cr–CrS cermets has been investigated. Although thermodynamics predicts that 200 % excess Cr is the upper limit on the Cr content that permits a self-sustained reaction to occur, in this study the synthesis of the cermets was demonstrated to be possible for a Cr:S molar ratio of up to four times the stoichiometric value.

Mechanical properties were measured as a function of Cr:S molar ratio. Quasi-static properties demonstrate the role of chromium addition, which leads to an overall improvement of the mechanical properties of the fabricated cermets. Statistical analysis was performed using one-way ANOVA. P values less than 0.05 were considered to be statistically significant in all tests. The differences in means of each group were analyzed by analysis of variance (ANOVA) with microhardness, flexural strength and fracture toughness as the dependent variables, and the Cr:S molar ratio (chromium content) as the independent factor. ANOVA exhibited highly significant differences among the tested composite materials for the mean values of microhardness ($p < 0.005$), flexural strength ($p < 0.01$), and fracture toughness ($p < 0.05$).

According to the manufacturing process of Cr–CrS cermets that we conducted and described here, it is possible to make these cermets as functionally graded materials, because they can be cast layer by layer with different compositions (various Cr contents) in a mold with desirable final shape of the article. Harder inclusions with different geometries and volumes (such as boron carbide or silicon carbide) also can be embedded into sulfide ceramics during the SHS process making a hybrid composite with applications as a material for ballistic armor.

Acknowledgements This Project was supported under NSERC Strategic Grant “Design and Net-shape Manufacturing of Hybrid Composites for Ballistic Protection” with Francois Barthelat serving as principal investigator. The authors would like to thank Deju Zhu for his contributions in mechanical characterization methods. The authors also appreciate the effort of Alexander Capozzi for his input regarding the synthesis of chromium sulfide samples.

References

1. Fu Z, Wang H, Wang W, Yuan R, Munir Z (1992) Process of study on self-propagating high-temperature synthesis of ceramic–metal composites. Int J SHS 2(175):1993a
2. Jones DR, Ashby MF (1998) Engineering materials volume 2: an introduction to microstructures, processing and design, 2nd edn. Butterworth-Heinemann, Oxford
3. Davis JR (1990) ASM Handbook: Properties and selection: nonferrous alloys and special-purpose materials, vol 2. ASM International, Material Park, OH
4. Moya JS, Lopez-Esteban S, Pecharromán C (2007) The challenge of ceramic/metal microcomposites and nanocomposites. Prog Mater Sci 52(7):1017–1090
5. Rodriguez-Suarez T, Bartolomé J, Moya J (2012) Mechanical and tribological properties of ceramic/metal composites: a review of phenomena spanning from the nanometer to the micrometer length scale. J Eur Ceram Soc 32(15):3887–3898
6. Behl WK, Plichta EJ (1995) Cathode material for use in a high temperature rechargeable molten salt cell and high temperature rechargeable molten salt cell including the cathode material. Google Patents
7. Mizera MA (1997) Ignition temperature measurements of metallic sulfides in SHS processes. M. Eng thesis, McGill University
8. Jellinek F (1957) The structures of the chromium sulphides. Acta Crystallogr 10(10):620–628
9. Mrowec S, Zastawnik M (1966) On the defect structure of chromium sulphide. J Phys Chem Sol 27(6):1027–1030
10. Gershinsky G, Haik O, Salitra G, Grinblat J, Levi E, Daniel Nessim G, Zinigrad E, Aurbach D (2012) Ultra fast elemental synthesis of high yield copper Chevrel phase with high electrochemical performance. J Sol State Chem 188:50–58
11. Holleck G, Driscoll J (1977) Transition metal sulfides as cathodes for secondary lithium batteries—II. titanium sulfides. Electrochim Acta 22(6):647–655
12. Richardson JT (1988) Electronic properties of unsupported cobalt-promoted molybdenum sulfide. J Catal 112(1):313–319
13. Tada H, Fujishima M, Kobayashi H (2011) Photodeposition of metal sulfide quantum dots on titanium (IV) dioxide and the

applications to solar energy conversion. Chem Soc Rev 40(7): 4232–4243
14. Kouzu M, Uchida K, Kuriki Y, Ikazaki F (2004) Micro-crystalline molybdenum sulfide prepared by mechanical milling as an unsupported model catalyst for the hydrodesulfurization of diesel fuel. Appl Catal A 276(1):241–249
15. Daage M, Chianelli R, Ruppert A (1993) Structure-function relations in layered transition metal sulfide catalysts. Stud Surf Sci Catal 75:571–584
16. Jacobsen CJ, Törnqvist E, Topsøe H (1999) HDS, HDN and HYD activities and temperature-programmed reduction of unsupported transition metal sulfides. Catal Lett 63(3–4):179–183
17. Tomoshige R, Niitsu K, Sekiguchi T, Oikawa K, Ishida K (2009) Some tribological properties of SHS-produced chromium sulfide. Int J Self-Propagating High-Temp Synth 18(4):287–292
18. Ikorskii V, Doronina L, Batsanov S (1973) Magnetic properties of chromium sulfide selenides and sulfides. J Struct Chem 14(1):145–148
19. Bongers P, Van Bruggen C, Koopstra J, Omloo W, Wiegers G, Jellinek F (1968) Structures and magnetic properties of some metal (I) chromium (III) sulfides and selenides. J Phys Chem Sol 29(6):977–984
20. Nabavi A, Capozzi A, Goroshin S, Frost D, Barthelat F (2014) A novel method for net-shape manufacturing of metal-metal sulfide cermets. J Mater Sci 49(23):8095–8106. doi:10.1007/s10853-014-8517-4
21. Zhang W, Wang H, Wang P, Zhang J, He L, Jiang Q (2008) Effect of Cr content on the SHS reaction of Cr–Ti–C system. J Alloys Compd 465(1):127–131
22. Merzhanov AG (2004) The chemistry of self-propagating high-temperature synthesis. J Mater Chem 14(12):1779–1786
23. Munir Z (1993) Analysis of the origin of porosity in combustion synthesized materials. J Mater Synth Process 1(6):387–394
24. Munir ZA, Anselmi-Tamburini U (1989) Self-propagating exothermic reactions: the synthesis of high-temperature materials by combustion. Mater Sci Rep 3(7):277–365
25. Bale C, Chartrand P, Degterov S, Eriksson G, Hack K, Ben Mahfoud R, Melançon J, Pelton A, Petersen S (2002) FactSage thermochemical software and databases. Calphad 26(2):189–228
26. ASTM Standard E 562-02: standard test method for determining volume fraction by systematic manual point count (2002). ASTM International, West Conshohocken, PA, EUA
27. Waldner P, Sitte W (2011) Thermodynamic modeling of the Cr–S system. Int J Mater Res 102(10):1216–1225
28. Goldstein J, Newbury DE, Joy DC, Lyman CE, Echlin P, Lifshin E, Sawyer L, Michael JR (2003) Scanning electron microscopy and X-ray microanalysis. Springer, New York
29. Guy AG, Bever M, Hench L, Peterlin A (1972) Introduction to materials science. McGraw-Hill, New York
30. Bartolomé J, Beltrán J, Gutiérrez-González C, Pecharromán C, Muñoz M, Moya J (2008) Influence of ceramic–metal interface adhesion on crack growth resistance of ZrO_2–Nb ceramic matrix composites. Acta Mater 56(14):3358–3366
31. Ashby MF (2011) Chapter 4—Material Property Charts. In: Ashby MF (ed) Materials selection in mechanical design, 4th edn. Butterworth-Heinemann, Oxford, pp 57–96
32. Schutz R, Watkins H (1998) Recent developments in titanium alloy application in the energy industry. Mater Sci Eng 243(1):305–315